UNIABUJA Journal of Engineering and Technology

https://ujet.uniabuja.edu.ng/

ISSN: 2714-3236 (Online); 2714-3228 (Print)

Volume 3, Issue 1, 2025; 50-57

Influence of Deposition Parameters on the Mechanical Performance of Ti/TiN Coatings on Ti–51 at% Ni Alloy

Ishiaka S. ARUDI[1*], Abdulhakeem H. NURUDEEN[1], Abraham H. ABUAH[1]

[1]*Department of Mechanical Engineering, University of Abuja, Abuja, Nigeria*

*shuaibu.ishiaka@uniabuja.edu.ng

Abstract

The Ti–51 at% Ni shape-memory alloy demonstrates remarkable functional attributes, including resistance to corrosion, pronounced pseudoelasticity, and high mechanical strength. Nonetheless, concerns regarding its biocompatibility arise due to the potential release of nickel ions during biomedical implantation. To address this limitation, the present investigation focused on optimizing Ti/TiN surface coatings on the alloy. Such coatings are anticipated to enhance the alloy's surface integrity, particularly by increasing hardness to withstand external loading conditions. Moreover, achieving robust adhesion of the deposited layers is essential to mitigate any adverse effects associated with metallic ion release. Experimental analysis revealed that maximum adhesion strength was attained under processing conditions of 370 W DC power, 100 °C substrate temperature, 50 V bias voltage, and 5 sccm nitrogen flow. In contrast, peak hardness was observed at 370 W DC power, 150 °C, 75 V bias voltage, and 5 sccm nitrogen flow. Subsequent validation confirmed a 46.5% improvement in hardness, accompanied by a 9.7% increase in adhesion strength, thereby demonstrating effective bonding of the coatings to the alloy substrate. These findings establish a foundation for future research into the application of surface coatings to enhance the biocompatibility of titanium-based alloys.

Keywords: *DC magnetron sputtering, Ti/TiN coating, Process parameter, optimization, characterization.*

1.0 Introduction

Titanium–nickel alloys with a nickel concentration in the range of 48–51 at% are distinguished by their exceptional resistance to corrosive environments and their ability to recover original form after deformation. These functional attributes arise from the intrinsic shape-memory phenomenon and pronounced superelastic response, which collectively underpin their extensive utilization in biomedical and clinical applications (Chen & Thouas, 2015; Shayesteh Moghaddam et al., 2016) The shape-memory response of Ti–Ni alloys imparts exceptional mechanical adaptability, allowing the material to revert to its initial geometry following applied stress. Notably, these alloys can recover strains of up to 8% when subjected to physiological temperatures near 37 °C. Such performance characteristics closely mirror the mechanical behavior observed in natural biomaterials, particularly osseous tissue, underscoring their relevance in biomedical applications (Bandyopadhyay et al., 2023). However, there are apprehensions about the materials employed in biomedical applications, as the release of Ni-ions may provoke hypersensitivity in the human body (Chen & Thouas, 2015; Wilson, 2018).

Extensive scientific studies have explored the biocompatibility of titanium–nickel alloys. Their ability to resist corrosion and maintain compatibility within biological environments is largely attributed to the spontaneous development and strong adherence of a protective titanium dioxide (TiO_2) layer on the alloy surface (Shabalovskaya & Anderegg, 1995). The layer's fragility and thickness make it prone to fracture and delamination (Li et al., 2008). To mitigate these limitations, several surface modifications of Ti-Ni, including as physical vapour deposition (PVD) (Shabalovskaya & Anderegg, 1995; Wilson, 2018), ion implantation, and thermal spraying (Li et al., 2008; Meisner et al., 2018), are utilised to improve the surface properties of Ti-Ni. Surface modification techniques have been shown to markedly enhance the mechanical and chemical performance of alloys, yielding superior hardness, improved resistance to corrosive media, and greater wear durability. Among these approaches, physical vapor deposition (PVD) via magnetron sputtering is particularly advantageous, as it enables coating deposition at relatively moderate substrate temperatures in the range of 200–400 °C, producing films with thicknesses typically between 0.5 µm and 3.0 µm (Miletić et al., 2014; Subramanian et al., 1993). Delamination may arise in the coated implant due to inadequate adhesion, ultimately undermining the implant's effectiveness and durability (Di Bucchianico et al., 2018; Wilson, 2018). In biomedical implant applications, surface modification plays a critical role in mitigating issues such as delamination, wear, and other deposition-related defects. Among the available treatments, titanium nitride (TiN) coatings are particularly advantageous, as they significantly enhance the mechanical and chemical

Received: 13-09-2025 / Accepted: 19-10-2025 / Published: 24-12-2025

https://doi.org/10.70118/ujet.2025.0301.06

stability of the substrate. Specifically, TiN contributes to increased surface hardness, superior resistance to corrosive environments, improved wear performance, and greater protection against oxidative degradation (Li et al., 2008). Residual stresses regularly undermine the mechanical properties of TiN coatings on substrates (Meisner et al., 2018). In this context, Ti is commonly utilised as an interlayer between TiN and the substrate, which reduces and alleviates residual stress inside the Ti/TiN layer (Tang et al., 2011).

2.0 Materials and Methods

The Ti–51 at% Ni alloy, fabricated in 3 mm thick sheets and hereafter designated as the substrate, was procured from Stanford Advanced Materials, USA. Prior to coating, the specimens underwent sequential grinding on silicon carbide papers ranging from grit 220 to 4000 under a controlled water stream, in accordance with established preparation protocols. This was followed by fine polishing using a cloth impregnated with colloidal silica suspension to achieve a reflective, mirror-like finish. Surface topography was subsequently characterized using the SJ-310 Mitutoyo roughness tester (Japan), which indicated an average roughness below 0.1 µm. Such meticulous preparation is expected to facilitate uniform deposition and improved adhesion of sputtered coatings (Dai & Shi, 2021; Liu et al., 2014). The prepared substrates underwent ultrasonic cleaning in acetone for a duration of 10 minutes at 40 °C, after which they were sequentially rinsed with ethanol and deionized water before being air-dried under ambient laboratory conditions. This cleaning protocol was implemented to effectively remove residual contaminants and to enhance the chemical activity of the surface, thereby promoting the formation of robust interfacial bonds during subsequent processing.

2.1. Experimental Design

The experimental framework required a defined set of process parameters, which are summarized in Table 1. The variables systematically investigated during the coating trials included substrate temperature, applied direct current (DC) power, bias voltage, and the rate of nitrogen gas flow.

Table 1: Parameters used to deposit Ti/TN

Parameters	**Levels**		
	1	**2**	**3**
Power (W)	300	370	440
Temperature (^{o}C)	100	150	200
Bias voltage (V)	50	75	100
Nitrogen flow rate (sccm)	5	6	7

2.2 Coating Process

The Ti/TiN coatings on the Ti–51 at% Ni alloy was fabricated using a DC magnetron sputtering system housed at the Surface Engineering Laboratory, University of Malaya, Malaysia. The apparatus was configured in a vertical orientation, with the substrate stage positioned 12 cm beneath the DC and RF target holders, as illustrated in Fig. 1. For these experiments, a high-purity titanium disc (99.99%), 101.6 mm in diameter and 3 mm thick, was mounted on the DC target holder. The deposition sequence commenced by evacuating the chamber to a base pressure of 2.85×10^{-5} Torr, after which argon gas was introduced to stabilize the working pressure at 4.5×10^{-3} Torr. The substrates were then gradually heated to the designated temperatures. A titanium interlayer was first deposited by sputtering the Ti target for 60 minutes, followed by TiN deposition in a mixed nitrogen–argon atmosphere for 240 minutes. Upon completion of the coating process, the chamber was cooled to ambient conditions, and the coated specimens were retrieved for subsequent characterization.

Received: 13-09-2025 / Accepted: 19-10-2025 / Published: 24-12-2025

https://doi.org/10.70118/ujet.2025.0301.06

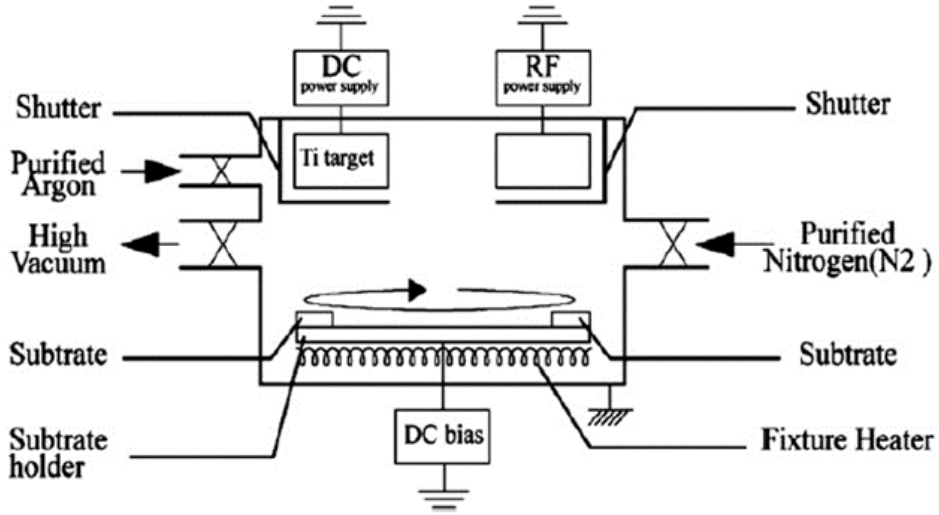

Figure 1: PVD device schematic diagram used in the experiment

2.3 Material Characterization

The microstructural features, elemental distribution, and coating thickness of the specimens were characterized using field emission scanning electron microscopy coupled with energy-dispersive X-ray spectroscopy (FESEM/EDX, ZEISS SIGMA 300 VP). Phase identification and crystallographic analysis were performed via X-ray diffraction (Rigaku Smart Lab XRD) under operating conditions of 40 kV tube voltage and 30 mA tube current, employing monochromatic $CuK\alpha_1$ radiation ($\lambda = 1.5406$ Å). The diffraction scans were conducted over a 2θ range of 30°–90°, with a step size of 0.10° and a grazing incidence angle of 1°.

Mechanical characterization was carried out using a Vickers microhardness tester (Shimadzu HMV-2 Series). Indentation was performed with a square-based diamond pyramid indenter (apex angle 136°) under a minimum load of 98.07 mN applied for 5 s. Measurements were repeated at three distinct points on each specimen, and the mean Vickers hardness value was reported (Arudi et al., 2023).

Adhesion performance was evaluated through scratch testing, a quantitative method for assessing coating integrity and interfacial reliability. The test was conducted using a Micro Material NanoTest system (Wrexham, UK) equipped with a 25 µm sphero-conical diamond stylus. A single horizontal scratch was applied under a maximum load of 3000 mN, with a track length of 1000 µm and a loading rate of 3 mN. The critical load (Lc_2), corresponding to complete coating failure, was used to determine adhesive strength, while the lower critical load (Lc) was defined as the onset of significant damage or a sharp increase in friction coefficient. Coating failure was further confirmed by correlating depth–distance profiles with optical micrographs obtained using an Olympus BX 61 microscope (Ali et al., 2006; Ozan et al., 2020).

3.0 Results and discussion

Prior to coating, the Ti–51 at% Ni alloy exhibited a baseline hardness of 184 ± 47 HV. Following deposition, the coated specimens demonstrated an average hardness of 332 ± 55 HV0.2 and an adhesion strength of 2709 ± 855 mN. The scratch test results, presented in Figure 2, revealed both cohesive failure (Lc_1) and adhesive failure occurring at a track length of approximately 679.98 µm, with a critical load (Lc_2) measured at 2174.96 mN. Coating failure was identified by correlating the critical load with the onset of delamination, as evidenced by the abrupt change in the depth profile coinciding with coating separation in the optical micrograph. The depth–distance curve was further compared with the scratch track image, where the plotted line denotes the point at which coating failure initiates.

Received: 13-09-2025 / Accepted: 19-10-2025 / Published: 24-12-2025

https://doi.org/10.70118/ujet.2025.0301.06

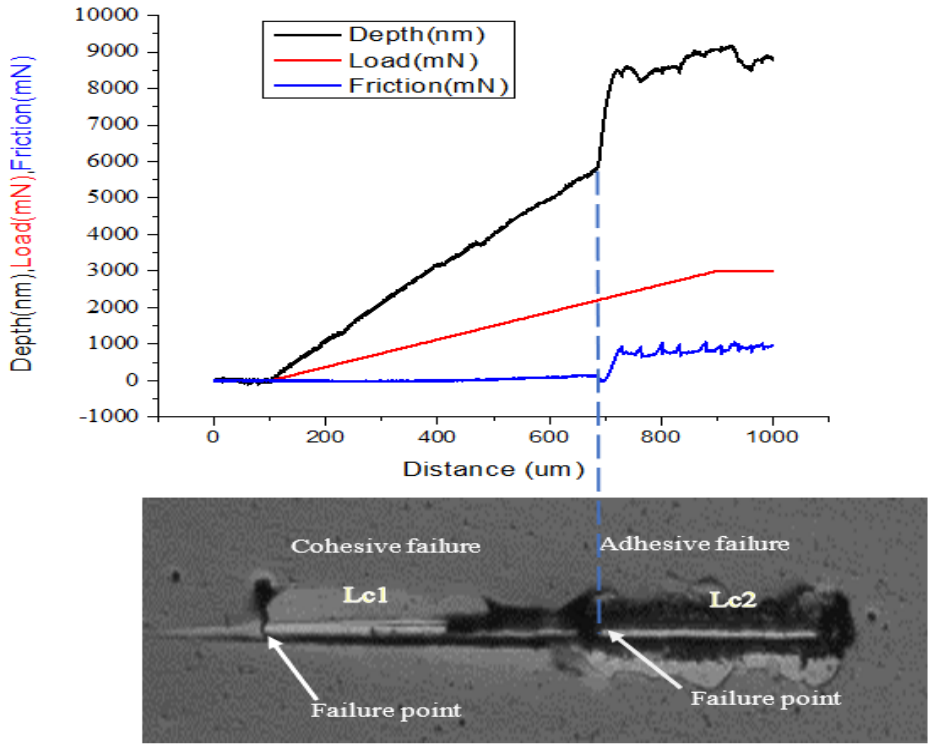

Figure 2: Profiles of depth and load against scratch distance

Elevating the nitrogen flow rate results in an increase in chamber pressure, which in turn enhances the sputtering kinetics. This effect is attributed to the greater population of ionized species generated within the plasma, thereby accelerating the deposition process. (Subramanian et al., 1993; Zaman & Meletis, 2017). On the other hand, a higher concentration of nitrogen in the chamber elevates the probability of collisions between gas-phase atoms and the sputtered species en route to the substrate. This increased interaction arises from the substantial presence of nitrogen atoms, which can influence the trajectory and energy of the depositing particles. (Dai & Shi, 2021). The free movement of nitrogen atoms within the chamber is restricted by frequent collisions, which consequently lowers the deposition rate. Conversely, reducing the nitrogen flow decreases the chamber pressure, thereby facilitating the unhindered transport of sputtered species and gas atoms toward the substrate, resulting in a higher deposition rate. At elevated chamber pressures, the kinetic energy of the sputtered particles is diminished, favoring the incorporation of positively charged species onto the substrate surface during film growth (Starosvetsky & Gotman, 2001). At applied powers of 300 W and 370 W, the ionized and sputtered particles acquire greater kinetic energy, which enhances the sputtering efficiency. This increase in deposition rate contributes to improved mechanical performance, reflected in higher scratch resistance and surface hardness. In contrast, when the power is raised to 440 W, the elevated energy input intensifies collision events between chamber gas atoms and sputtered species. The resulting scattering diminishes the effective sputtering rate, thereby reducing both the scratch force and the hardness of the coated surface.

The influence of substrate temperature on both scratch resistance and surface hardness was found to be relatively minor when compared with other deposition parameters. Interestingly, coatings processed at 100 °C exhibited higher scratch forces than those prepared at 150 °C and 200. This behavior is likely associated with the reduction in chamber gas pressure at elevated temperatures, which alters the deposition dynamics (Abbas et al., 2021). An increase in substrate temperature from 100 °C to 150 °C was accompanied by a rise in hardness; however, a further elevation to 200 °C resulted in a decline, most likely due to reduced atomic mobility at higher temperatures. The investigation also revealed that applying a bias voltage of 50 V enhanced the scratch resistance of the coating. In contrast, increasing the bias voltage to 75 V and 100 V led to a reduction in scratch force, which can be attributed to the generation of structural defects within the film caused by excessive ion bombardment (Arudi et al., 2023). The hardness of the TiN coating exhibited an upward trend as the bias voltage was raised from 50 V to 75 V. However, a further increase to 100 V resulted in a decline in hardness, which can be attributed to the re-sputtering of weakly bonded surface atoms under intensified ion bombardment (Dai & Shi, 2021; Sun et al., 2011).

3.3 Characterisation of the improved coated samples

X-ray diffraction analysis was employed to investigate the phase composition and crystallinity of the Ti/TiN coatings under different substrate temperatures and bias voltages, as presented in Figure 3. The results

Received: 13-09-2025 / Accepted: 19-10-2025 / Published: 24-12-2025

https://doi.org/10.70118/ujet.2025.0301.06

confirmed the formation of a uniform coating, with TiN diffraction peaks observed at 36.61° (111), 42.53° (200), 61.90° (220), 74.00° (311), and 77.31° (222) in Figure 3(a), and at 36.52° (111), 42.50° (200), 61.73° (220), and 73.90° (311) in Figure 3(b). These findings are in agreement with previously reported studies, thereby validating the consistency of the coating structure (X. Li et al., 2025; Zaman & Meletis, 2017). The diffraction patterns clearly confirm that the TiN coating crystallizes in a face-centered cubic (FCC) structure, with no secondary phases detected. The films are indexed to the space group Fm-3m (No. 225), with lattice constants of $a = b = c = 4.245$ Å (ICDD reference card 01-087-0626, Figure 5a) and $a = b = c = 4.251$ Å (ICDD reference card 03-065-5759, Figure 5b).

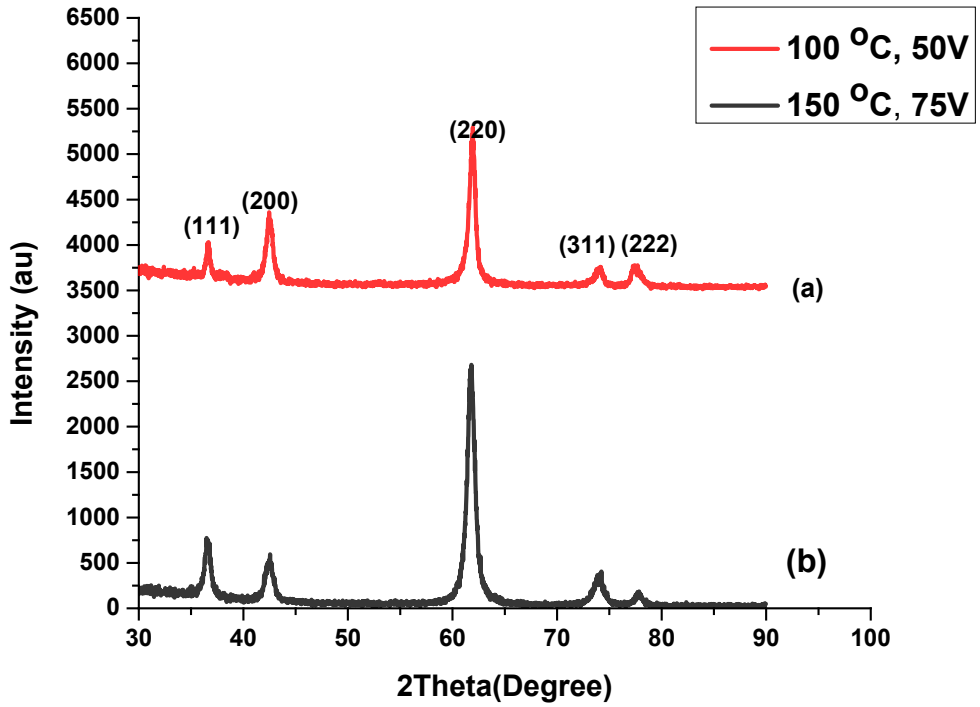

Figure 3: The XRD patterns of Ti/TiN coatings: (a) 370 W, 75 V, 5 sccm, 150 °C, (b) 370 W, 50 V, 5 sccm, 100 °C

Figure 5 reveals that the (220) reflection represents the dominant preferred orientation, indicating that the ion energy during deposition was sufficiently high. In contrast, the diminished intensity of the (111) peak in Figure 5(a) corresponds to deposition at 100 °C and a bias voltage of 50 V, whereas the stronger (111) peak observed at 150 °C and 75 V in Figure 3(b) reflects the influence of elevated substrate temperature. Under these conditions, the effect of gas pressure becomes negligible, as the increased atomic mobility allows energetic species to move freely across the substrate surface. The lower intensity of the (200) peak in Figure 3(b) is attributed to reduced surface free energy, which results from enhanced adatom mobility at higher temperatures and bias voltages (Dai & Shi, 2021; Fadlallah et al., 2014). The diffraction data indicate that the (222) reflection exhibits a decline in peak intensity as both substrate temperature and bias voltage increase, mirroring the behavior observed for the (200) plane. In contrast, the (311) peak intensity rises under the same conditions, following a trend comparable to that of the (111) and (220) orientations.

Figure 4 presents FESEM micrographs of the Ti/TiN-coated specimens, revealing a consistent pyramid-like surface morphology. Although the overall structural features are similar, variations in crystal grain size are evident between Figures 4(a) and 4(b), reflecting the influence of different substrate temperatures and bias voltages. The emergence of this pyramidal morphology is attributed to preferential growth along the (220) crystallographic plane, as corroborated by the XRD results.

The FESEM observations in Figure 4 reveal that all coatings exhibit a uniform particle size distribution, with densely packed grains and no discernible porosity. Variations in grain dimensions are directly linked to deposition parameters such as substrate temperature and applied bias voltage. As shown in Figure 3(a), the intensity of the (220) diffraction peak increases when the deposition conditions shift from 100 °C and 50 V to 150 °C and 75 V. This behavior reflects the combined effects of enhanced ion bombardment at higher bias voltages and increased adatom mobility at elevated temperatures, both of which promote crystalline film growth. With improved crystallinity, the grain size becomes larger, as evident at ×2500 magnification in Figure 6 (Arudi et al., 2023)

Received: 13-09-2025 / Accepted: 19-10-2025 / Published: 24-12-2025

https://doi.org/10.70118/ujet.2025.0301.06

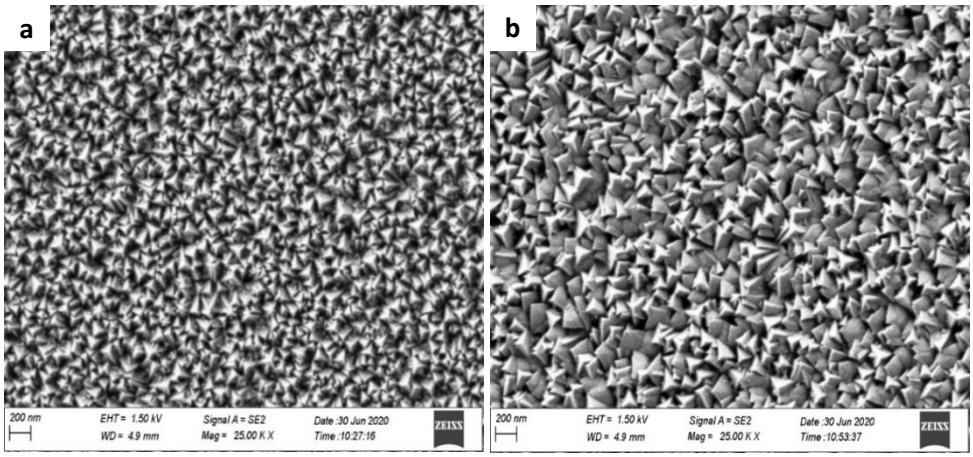

Figure 4: The FESEM surface morphology of Ti/TiN coating at: (a) 50 V and 100 °C, (b) 75 V and 150 °C

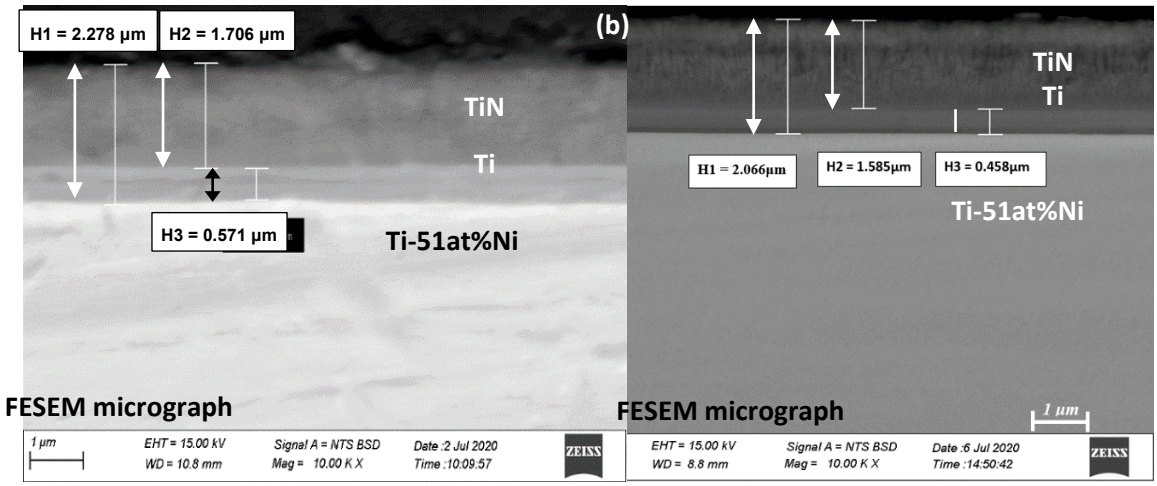

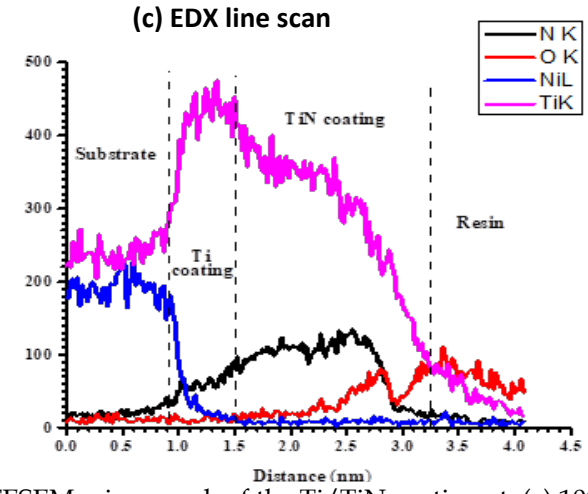

Figure 5: Cross-sectional FESEM micrograph of the Ti/TiN coating at: (a) 100 °C, 50 V (b) 150 °C, 75 V (c) EDX line scan along the cross-section

Figures 5(a) and 5(b) present cross-sectional FESEM images of Ti/TiN coatings deposited at 100 °C, 50 V and 150 °C, 75 V, respectively. In both cases, the coatings display a compact microstructure, free from cracks or interfacial voids between the film and the substrate. The cross-sectional analysis further indicates that variations in deposition parameters lead to differences in coating thickness. The EDX line scan shown in Figure 5(c) confirms the incorporation of nitrogen into the Ti interlayer. Increasing nitrogen incorporation is generally associated with enhanced hardness of the Ti interlayer, reflecting the strengthening effect of nitrogen doping (Ali et al., 2006; Liu et al., 2014; Mubarak et al., 2005).

The incorporation of nitrogen into the Ti interlayer enhances its mechanical integrity, thereby providing stronger support for the overlying TiN film and contributing to an increase in scratch resistance. This

Received: 13-09-2025 / Accepted: 19-10-2025 / Published: 24-12-2025

https://doi.org/10.70118/ujet.2025.0301.06

improvement is linked to the strengthening effect of nitrogen and the disruption of the native oxide layer on the substrate surface, facilitated by oxygen absorption within the Ti interlayer. However, when nitrogen concentration continues to rise beyond the optimal level, the interlayer becomes excessively brittle, reducing its ability to withstand interfacial stresses. As illustrated in Figure 2, this brittleness manifests as a decline in scratch force.

4.0 Conclusion

This study experimentally examined the deposition of Ti/TiN coatings on a Ti–51 at% Ni substrate using DC magnetron sputtering, with deposition parameters varied across direct current power, substrate temperature, bias voltage, and nitrogen flow rate. The key findings are summarized as follows:

- Scratch adhesion strength was maximized under conditions of 370 W, 100 °C, 50 V, and 5 sccm nitrogen flow.
- Hardness reached its highest value at 370 W, 150 °C, 75 V, and 5 sccm nitrogen flow.
- The introduction of a titanium interlayer prior to TiN deposition improved mechanical performance, yielding an approximate 10% increase in scratch adhesion strength and a 46.51% enhancement in hardness.
- The optimized combination of deposition parameters and interlayer design produced coatings with superior mechanical integrity, highlighting Ti/TiN films as promising candidates for biomaterial applications.

Finally, the results demonstrate that careful control of sputtering conditions and interlayer engineering can significantly influence coating performance. These findings provide a foundation for further investigations into the mechanical reliability and biocompatibility of Ti/TiN-coated Ti–Ni alloys for advanced biomedical use.

Conflict of Interest

The authors of this paper declare no conflict of interest in the publication of this paper.

References

Abbas, A., Hung, H.-Y., Lin, P.-C., Yang, K.-C., Chen, M.-C., Lin, H.-C., & Han, Y.-Y. (2021). Atomic layer deposited TiO2 films on an equiatomic NiTi shape memory alloy for biomedical applications. *Journal of Alloys and Compounds*, *886*, 161282.

Ali, M., Hamzah, E. B., & HJ. MOHD TOFF, M. R. (2006). Effect of substrate bias voltage on the microstructural and mechanical properties of tin-coated HSS synthesized by capvd technique. *Surface Review and Letters*, *13*(05), 621–633.

Arudi, I. S., Hamzah, E., Mat Yajid, M. A., Bushroa, A. R., Munshi, S. M., Al-Ashhab, M. S., & Ibrahim, M. Z. (2023). Taguchi optimization of hardness and scratch adhesion strength of multilayer Ti/TiN coatings on Ti- 51 at%Ni alloy deposited via magnetron sputtering technique. *Journal of Materials Research and Technology*, *27*, 7664–7672. https://doi.org/10.1016/j.jmrt.2023.11.166

Bandyopadhyay, A., Mitra, I., Goodman, S. B., Kumar, M., & Bose, S. (2023). Improving biocompatibility for next generation of metallic implants. *Progress in Materials Science*, *133*, 101053.

Chen, Q., & Thouas, G. A. (2015). Metallic implant biomaterials. *Materials Science and Engineering: R: Reports*, *87*, 1–57.

Dai, W., & Shi, Y. (2021). Effect of bias voltage on microstructure and properties of tantalum nitride coatings deposited by RF magnetron sputtering. *Coatings*, *11*(8), 911.

Di Bucchianico, S., Gliga, A. R., Åkerlund, E., Skoglund, S., Wallinder, I. O., Fadeel, B., & Karlsson, H. L. (2018). Calcium-dependent cyto-and genotoxicity of nickel metal and nickel oxide nanoparticles in human lung cells. *Particle and Fibre Toxicology*, *15*(1), 32.

Fadlallah, S. A., El-Bagoury, N., El-Rab, S. M. F. G., Ahmed, R. A., & El-Ousamii, G. (2014). An overview of NiTi shape memory alloy: Corrosion resistance and antibacterial inhibition for dental application. *Journal of Alloys and Compounds*, *583*, 455–464.

Li, X., Yang, Y., Shen, H., Zhou, M., Huang, B., Cui, L., & Hao, S. (2025). Research progress on surface modification and coating technologies of biomedical NiTi alloys. *Colloids and Surfaces B: Biointerfaces*, 114496.

Li, Y., Wei, S., Cheng, X., Zhang, T., & Cheng, G. (2008). Corrosion behavior and surface characterization of tantalum implanted TiNi alloy. *Surface and Coatings Technology*, *202*(13), 3017–3022.

Liu, K.-Y., Lee, J.-W., & Wu, F.-B. (2014). Fabrication and tribological behavior of sputtering TaN coatings. *Surface and Coatings Technology*, *259*, 123–128.

Received: 13-09-2025 / Accepted: 19-10-2025 / Published: 24-12-2025

https://doi.org/10.70118/ujet.2025.0301.06

Meisner, S. N., Yakovlev, E. V, Semin, V. O., Meisner, L. L., Rotshtein, V. P., Neiman, A. A., & D'yachenko, F. (2018). Mechanical behavior of Ti-Ta-based surface alloy fabricated on TiNi SMA by pulsed electron-beam melting of film/substrate system. *Applied Surface Science*, *437*, 217–226.

Miletić, A., Terek, P., Kovačević, L., Vilotić, M., Kakaš, D., Škorić, B., & Kukuruzović, D. (2014). Influence of substrate roughness on adhesion of TiN coatings. *Journal of the Brazilian Society of Mechanical Sciences and Engineering*, *36*(2), 293–299.

Mubarak, A., Hamzah, E. B., Mohd Toff, M. R. H., & Hashim, A. H. Bin. (2005). The Effect of nitrogen gas flow rate on the properties of TiN-coated high-speed steel (HSS) using cathodic arc evaporation physical vapor deposition (PVD) technique. *Surface Review and Letters*, *12*(04), 631–643.

Ozan, S., Munir, K., Biesiekierski, A., Ipek, R., Li, Y., & Wen, C. (2020). Titanium alloys, including nitinol. In *Biomaterials Science* (pp. 229–247). Elsevier.

Shabalovskaya, S. A., & Anderegg, J. W. (1995). Surface spectroscopic characterization of TiNi nearly equiatomic shape memory alloys for implants. *Journal of Vacuum Science & Technology A: Vacuum, Surfaces, and Films CONF− 1*, *13*(5), 2624–2632.

Shayesteh Moghaddam, N., Taheri Andani, M., Amerinatanzi, A., Haberland, C., Huff, S., Miller, M., Elahinia, M., & Dean, D. (2016). Metals for bone implants: Safety, design, and efficacy. *Biomanufacturing Reviews*, *1*(1), 1.

Starosvetsky, D., & Gotman, I. (2001). TiN coating improves the corrosion behavior of superelastic NiTi surgical alloy. *Surface and Coatings Technology*, *148*(2–3), 268–276.

Subramanian, C., Strafford, K. N., Wilks, T. P., Ward, L. P., & McMillan, W. (1993). Influence of substrate roughness on the scratch adhesion of titanium nitride coatings. *Surface and Coatings Technology*, *62*(1–3), 529–535.

Sun, T., Wang, L., & Wang, M. (2011). (Ti, O)/Ti and (Ti, O, N)/Ti composite coatings fabricated via PIIID for the medical application of NiTi shape memory alloy. *Journal of Biomedical Materials Research Part B: Applied Biomaterials*, *96*(2), 249–260.

Tang, C. Y., Zhang, L. N., Wong, C. T., Chan, K. C., & Yue, T. M. (2011). Fabrication and characteristics of porous NiTi shape memory alloy synthesized by microwave sintering. *Materials Science and Engineering: A*, *528*(18), 6006–6011.

Wilson, J. (2018). Metallic biomaterials: State of the art and new challenges. *Fundamental Biomaterials: Metals*, 1–33.

Zaman, A., & Meletis, E. I. (2017). Microstructure and mechanical properties of TaN thin films prepared by reactive magnetron sputtering. *Coatings*, *7*(12), 209.

Received: 13-09-2025 / Accepted: 19-10-2025 / Published: 24-12-2025

https://doi.org/10.70118/ujet.2025.0301.06